

Simultaneous observation of melt flow and motion of equiaxed crystals during solidification using a dual phase Particle Image Velocimetry technique

This article has been downloaded from IOPscience. Please scroll down to see the full text article.

2012 IOP Conf. Ser.: Mater. Sci. Eng. 33 012042

(<http://iopscience.iop.org/1757-899X/33/1/012042>)

View [the table of contents for this issue](#), or go to the [journal homepage](#) for more

Download details:

IP Address: 178.191.204.136

The article was downloaded on 31/05/2013 at 10:24

Please note that [terms and conditions apply](#).

Simultaneous observation of melt flow and motion of equiaxed crystals during solidification using a dual phase Particle Image Velocimetry technique

A Kharicha, M Stefan-Kharicha, A Ludwig and M Wu

Chair for Simulation and Modelling of Metallurgical Processes, Dept. of Metallurgy, University of Leoben, A-8700 Leoben, Austria

E-mail: abdellah.kharicha@mu-leoben.at

Abstract. A dual phase Particle Image Velocimetry (PIV) technique is applied to study the flow and coupled equiaxed-columnar solidification in an ingot of $\text{NH}_4\text{Cl-H}_2\text{O}$ solution. This technique is able to monitor simultaneously both velocities of the liquid flow and motion of equiaxed crystals. Before solidification started, a stable thermal buoyancy driven flow, laminar and 2D, was initialized in the ingot. As soon as solidification began, solutal buoyancy together with falling crystals destabilized the initial laminar flow into multiple chaotic cells, and a 3D turbulent regime was achieved. The kinetic energy for the flow was calculated. The interaction between the equiaxed grains and the melt flow was analyzed according to relative velocities. The settling velocity of an isolated equiaxed crystal was found to be 41 times smaller than the calculated one of a spherical crystal of equivalent size. The coupling between the fluid flow and the equiaxed crystal was found to be important in area of high crystal density. Chaotic and turbulent behaviors were found to be damped in regions of high equiaxed crystal density.

1. Introduction

Solidification is a multi-disciplinary field involving thermodynamics, fluid dynamics and solid mechanics, heat and mass transfer, and other disciplines [1-3]. Most challenging problems in solidification modeling are the complex interactions between physical phenomena occurring at different length scales ranging from atomic rearrangement over single crystal-melt interactions, to heat extraction, momentum and species transport at the system level.

Due to its transparency, $\text{NH}_4\text{Cl-H}_2\text{O}$ solution was used for many experimental studies in the past [1-4], as the perfect analogue for solidification of metallic alloys.

The Particle Image Velocimetry (PIV) technique used here, for distinguishing between the two different signals, employs fluorescent tracer particles [5, 6]. The fluorescent tracers scatter the light at a wavelength different from that scattered by the equiaxed crystals. The use of two cameras is necessary. The first camera mounted with a green filter (band pass filter of 532 nm) detects only the laser light scattered by the equiaxed crystals. The second camera uses an orange filter (570 nm) through which the light reemitted by the fluorescent dye (Rhodamine B) can be recorded. This technique was successfully applied to two-phase water-bubble flows, with simultaneous separation and measurement of the different phases. Here it is applied to investigate the liquid and equiaxed crystal two phase flow.

2. Experimental Procedure

The experimental set-up is composed of: the test cell, the illumination system, the optics and the computer. The test cell (Figure 1) was cubic ($10 \times 10 \times 1 \text{ cm}^3$) with three sides made of brass, and commercial glass for the front and back; the upper part was open. The cast cell was cooled down homogeneously through the three brass walls. The illumination system was an Nd-Yag double pulsed



Figure 1. Rectangular cavity used for controlled solidification experiments. The inner dimensions are $10 \times 10 \times 1 \text{ cm}^3$.

laser and the optics were 2 CCD cameras mounted in parallel and perpendicular to the test cell. The laser and the CCD cameras were piloted by the computer via the commercial software FlowManager. A hypereutectic 29.5 wt.% $\text{NH}_4\text{Cl} - \text{H}_2\text{O}$ solution was solidified under controlled temperatures. The cooling rate was $1.2^\circ\text{C}/\text{min}$ for the brass walls. The liquid solution was poured into the cell at 45°C , after 30 min the cooling was started from 45°C until 5°C . The air temperature around the test cell was 24.7°C .

3. Results

The solidification process follows different stages. The first stage (labeled by TH) involved only liquid, whereas the last four (labeled by PTH, TU, CC, and MF) involved solidification as well.

3.1 Thermal stage (TH): stable thermal buoyancy

When the walls temperature decreases below the temperature of the solution, the liquid close to the vertical walls has a tendency to sink by thermal buoyancy. However, in the experiment it took 8 min. until a stable clockwise convection pattern established. The direction of the flow was downwards near the walls and upwards at the center (Figure 2). As cooling became stronger and stronger the magnitude of downwards flow velocity slightly increased with time. It is clear that the hydrodynamic pattern of this stage was found to be very stable and symmetric. Stage TH lasted only around 1-2 minutes before evidences for solidification appeared.

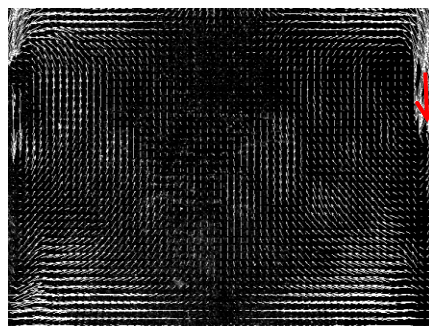


Figure 2. Stable thermal buoyancy stage at 8 min after the cooling started. The velocity vectors are linearly scaled between $v_{min} = 0.08 \text{ mm/s}$ and $v_{max} = 1.12 \text{ mm/s}$ (red arrow).

3.2 Perturbation of the thermal state (PTH): solidification perturbed thermal state

Visible solidification, mainly columnar, started at about 9-10 minutes after beginning of cooling. It did not appear uniformly all over the walls surface, but rather in islands of columnar dendritic crystals (Figure 3a). In the vicinity of each columnar island the flow is immediately disturbed by the presence of one or two small eddies (Figure 3b). However, during about the first 3-4 minutes of visible solidification, the main pattern of the flow (symmetry, magnitude, main direction) is not changed. Sometimes the strong downward jet is able to detach columnar structures of up to 5 mm in size from the cooling wall. This phenomenon happens mainly at this stage, rarely in later stages. Few equiaxed crystals were also occasionally observed at the vicinity of the vertical walls (Figure 3b). This stage lasted around 3-4 minutes.

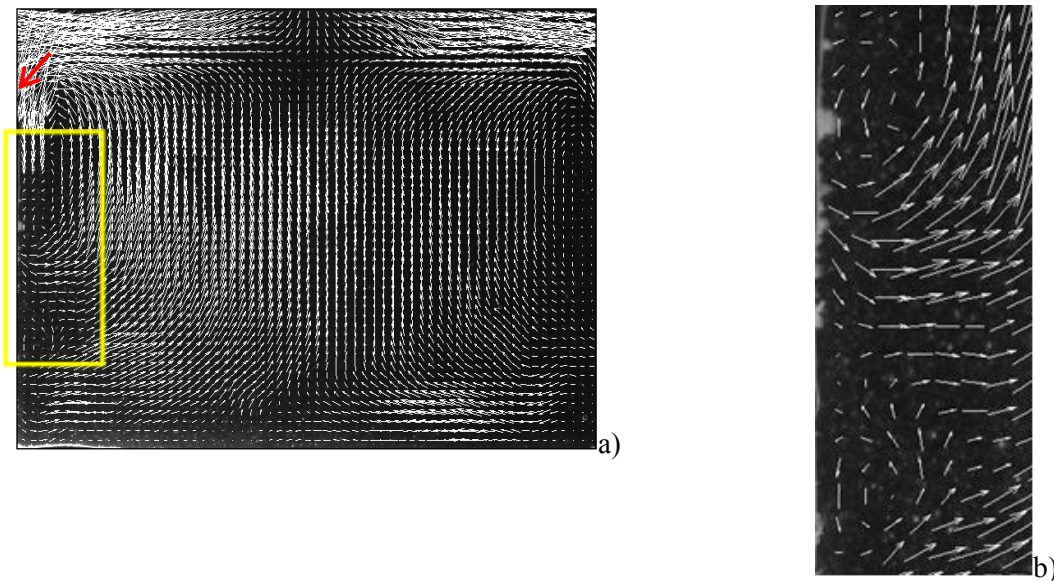


Figure 3. a) Perturbed thermal stage (PTH), at $t = 9$ min after switching on cooling. The velocity vectors were scaled between $v_{min} = 0.052$ mm/s and $v_{max} = 0.73$ mm/s (red arrow); b) zoom- in of yellow square.

3.3 Turbulent flow state (TU)

As the solidification proceeded, equiaxed crystals increased in number, and perturbations of the main flow increased in magnitude. A new flow regime with large number of small eddies appeared (Figure 4a-b). Now solidification covered totally the walls and filled about 5% of the picture (at the end ~30% is reached). The lack of coherence of the observed eddies, and the presence of strong velocity gradients even far from the walls, is a strong indication of the three dimensional and turbulent character of this regime. In this stage large visible equiaxed crystals appeared only near the walls. However, the movement of the small crystals could be evaluated by correlation. This stage lasted about 2 minutes.

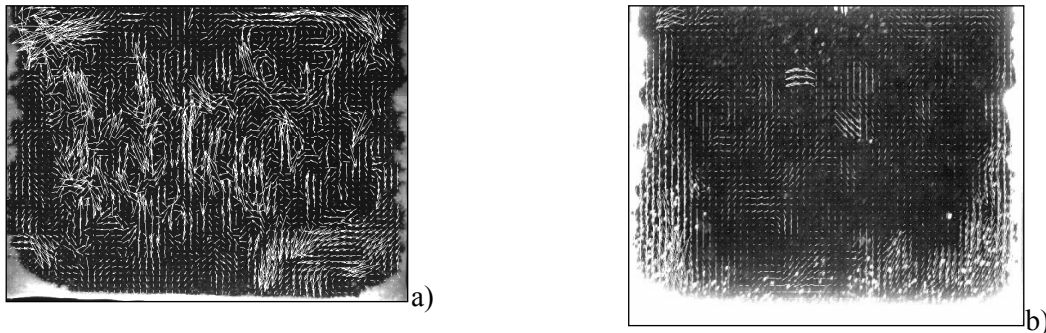


Figure 4. Turbulent regime (TU). The liquid velocity is shown in (a) and the velocity of the equiaxed crystals is shown in b), at $t = 13$ min. The velocity vectors are scaled between $v_{min} = 0.051$ mm/s and $v_{max} = 0.709$ mm/s for the liquid (a) and between $v_{min} = 0.252$ mm/s and $v_{max} = 3.52$ mm/s for the equiaxed crystals (b).

3.4 Coherent chaotic flow state (CC)

Out of the turbulent flow stage a regime where the flow map is coherent but still chaotic appeared (Figure 5a). The characteristic eddy size was of about 1.5-2 cm, and thus larger than the distance between the two glass plates. The equiaxed crystallization was very strong (Figure 5b), and the leading solidification mechanism. The velocity magnitude was at its maximum. Large crystals appeared even in the bulk far from the vertical walls, and often fell, grouped in columns, or in agglomeration. Note that during this stage most of the solidification process happened. This included the initiation and growth of freckles (flow channels in the mush) where traces can be seen in Figure 6a. At the end of this stage, the solidification front had almost reached its final position. Stage CC lasted about 10 minutes.

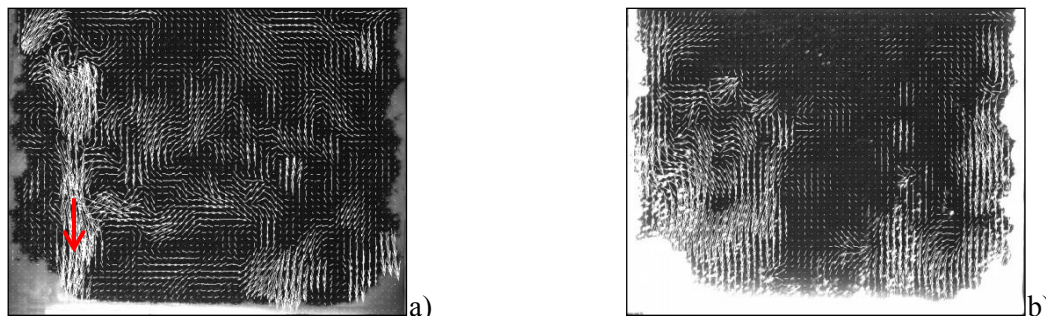


Figure 5. Examples showing the melt velocities (a) and the equiaxed crystals velocities (b), for the so-called coherent chaotic regime (CC). The two-camera PIV measurement was done at $t = 15$ min. The velocity vectors are scaled between $v_{min} = 0.111$ mm/s and $v_{max} = 1.56$ mm/s (red arrow) for the liquid (a) and between $v_{min} = 0.278$ mm/s and $v_{max} = 3.87$ mm/s for the equiaxed crystals (b).

3.5 Meandering flow state (MF): quasi-steady meandering flow occurs

The small eddies disappeared progressively and gave place to a meandering flow traveling from the top to the bottom (Figure 6a). The flow is stratified into 5 to 7 circulation layers. It is possible to follow the flow streamlines from the top to the bottom of the cell. The number density of equiaxed crystals decreased in the vicinity of the vertical solidification front, and increased in the bulk in the form of relatively large crystal column or in agglomeration (Figure 6b). But globally equiaxed falls were not as strong as in the previous CC regime. The meander flow seems to penetrate the bottom mushy zone. In this regime, the number of equiaxed crystals and the magnitude of the flow velocity were continuously decreasing in time until extinction. Finally about 30% of the cell volume is filled with solid. Stage MF lasted around 5-10 minutes until the typical meandering flow disappeared.

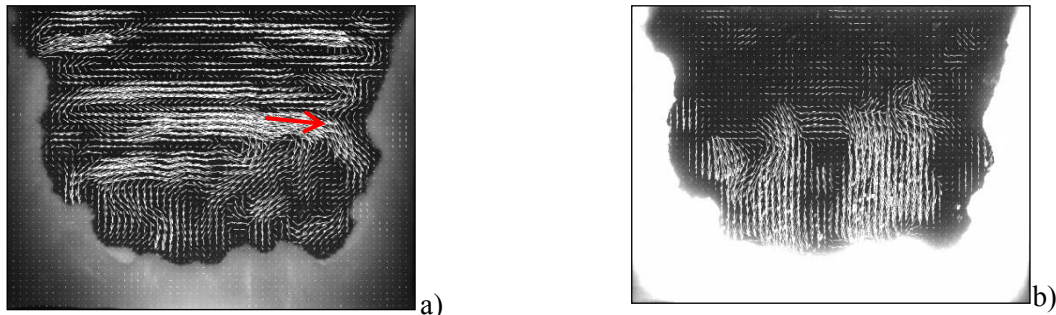


Figure 6. Examples showing the melt velocities (a) and the equiaxed crystals velocities (b) for the meandering flow regime (MF). The two-camera PIV measurement was done at $t = 30$ min. The velocity vectors are scaled between $v_{min} = 0.067$ mm/s and $v_{max} = 0.466$ mm/s (red arrow) for the liquid (a) and between $v_{min} = 0.155$ mm/s and $v_{max} = 2.17$ mm/s for the equiaxed crystals (b).

4 Analysis and Discussion

4.1 The evolution in time of the total kinetic energy of the liquid flow

The evolution in time of the total kinetic energy of the liquid flow calculated with the measured velocity magnitude U as

$$KE = \sum_N \frac{1}{2} U^2 \quad (1)$$

is presented in Figure 7. N represents the total number of vectors all over the surface cell and it is constant. When solidification happens the vectors in the mushy zone are zero. Although the presence of some instabilities, no large change in the kinetic energy is observed before the start of solidification. Even if we would have taken the large velocity jets along the walls, which are not completely resolved, into account the kinetic energy would not change dramatically.

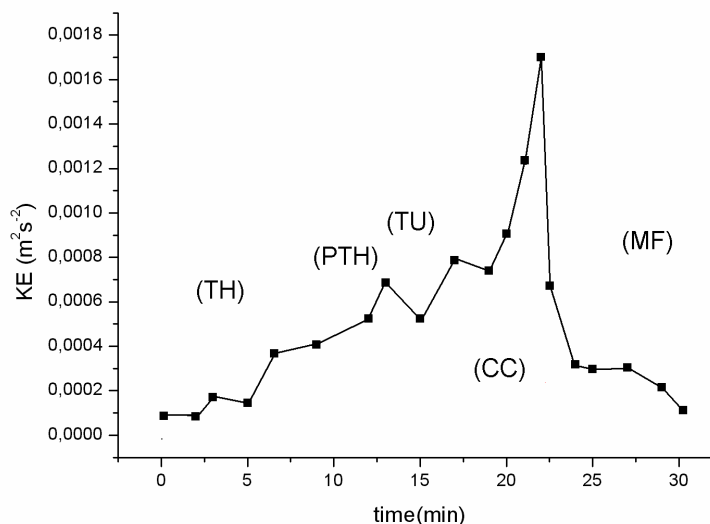


Figure 7. Evolution of the liquid kinetic energy, during the different flow regimes.

The kinetic energy increased continuously during the perturbed thermal and turbulent regimes. The maximum is reached close to the end of the coherent chaotic regime at about $t = 22$ minutes. Later, in

the stratified regime (MF) the kinetic energy decreases to levels similar to that of the thermal buoyancy states. This evolution of KE does not correspond to what is reported by Skudarnov [7], where the velocity decreases in magnitude all along with time. The reason for that might be the fact that in our experiment we end up in a partly solidified sample, where all dynamics fade out with time.

At around 25 minutes the lower number of equiaxed crystals promotes a steadier and slower melt flow structure (Figure 6a). However, the flow path seems to be controlled by the local curves of the dendrite tip envelop. It is probable that the meandering flow regime is created by an auto-organisation of the solutal convection in curved constrained geometry (from top to bottom). The concentration differences are small since the evolution of the dendrite tip envelop front is nearly stopped, but large enough to generate a flow with a KE similar to that of the thermal states.

4.2 Relative velocity

The relative velocity was estimated as the difference between measured crystal velocity and flow velocity. To obtain accurate crystal velocities it is necessary to choose an area where the number of crystals is large enough for the PIV correlation. The fundamental aspect is the relation between the relative velocity and the crystal size. Such a relation exists for spherical particles, and is known as Stoke's law. To check its validity for equiaxed crystals it is necessary to extract the relative velocity for isolated crystals, not in crystal agglomeration. In Figure 8 the calculated relative velocities of single crystals as function of the measured size are plotted. The maximum horizontal diameter of the crystal (d) was calculated from the pictures (1600*1186 pixels), by counting the number of bright pixels. Due to an overexposure of the pictures, necessary for a good PIV, the size of the crystals may be overestimated.

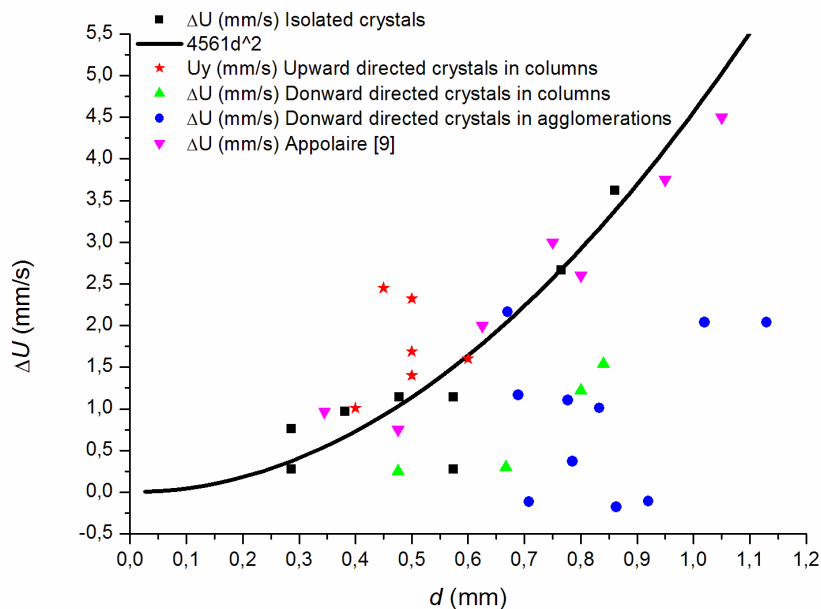


Figure 8. Relative velocity for single crystals versus the crystal size diameter (d), and comparison between rising (red) and falling (green) velocities magnitude in chimneys.

The results for isolated crystals show an increase of the relative velocity with the measured size. The magnitudes of the relative velocities found for corresponding sizes are very similar to those reported by Appolaire [8, 9]. The correlation follows a clear power tendency. Based on the Stokes's law the relative velocity of a compact sphere can be calculated by:

$$\Delta U = \frac{d^2 g}{18C_D \mu} (\rho_A - \rho_W) = \alpha \cdot d^2 \quad (2)$$

where ρ_A is the density of the sphere, ρ_W the density of the surrounding fluid, g the gravity constant, C_D the drag coefficient, μ the dynamic viscosity of the fluid and d is the diameter of the sphere. α gathers the materials properties in one single factor.

Using the measured sizes and velocities, the particle Reynolds number $Re_p = \rho_A \Delta U d / \mu$ is always smaller than 1, which allows the use of equation (2). Equation (2) was used to fit the experimental data of Figure 8. With the materials properties given in Table 1, the value of α can be calculated to be 188402.3. However, the fit to the measuring points from Figure 8 gives $\alpha = 4561$. Thus the computed relative velocity for spheres (0.1 m/s for $d = 0.75$ mm) is almost 41 times bigger than the measured ones.

Table 1: Material properties important for the discussion of the results

Property	Symbol	Value	Ref.
density of the liquid (water)	ρ_W	1078 kg·m ⁻³	Beckermann et al. [10]
density of solid ammonium chloride	ρ_A	1527.4 kg·m ⁻³	Rowe et al. [11]
dynamic viscosity of the liquid	μ	1.3×10^{-3} kg·m ⁻¹ ·s ⁻¹	Beckermann et al. [10]

Due to the fact that the equiaxed crystals are not spherically shaped, and to their rough fractal surface, it was expected that spheres have a larger relative velocity than the equiaxed crystals. This is the reason why numerical simulations were performed by using modified drag laws to account for the equiaxed shapes [12-15]. These drag laws, predict systematically larger drag coefficients ($C_D > 1$) than for spheres. In our case the drag coefficient is indeed larger and equal to 41.3.

Based on the experimental correction of equation (2) the equiaxed relaxation time is estimated to be:

$$\tau_e = \alpha \frac{\rho_A - \rho_W}{\rho_A} d^2 \leq 10^{-4} s \quad (3)$$

Compared to the measurement frequency (250 ms), it is very small. It can be assumed that the crystals reach instantaneously their terminal relative velocity. Thus, the polynomial increase of ΔU observed in Figure 8 can be directly related to the growth of volume during the crystal fall.

By comparing Figure 4a and Figure 4b, we can notice that variations of the liquid velocities are smoother in areas where a large number of equiaxed crystals exist. This phenomenon is particularly visible if we compare the flow coherence in the bulk with the high equiaxed density regions. The flow in these regions is well structured in clear streamlines or in large eddies. Obviously, the presence of crystals flows, through drag interaction, damps the turbulence eddies. We can suppose that due to the extension of the area of falling crystals and to the decrease in magnitude of ΔC , a laminarization of the entire domain occurs, leading to a transition to the laminar chaotic regime (Figure 5).

5 Conclusions

A special Particle Image Velocimetry (PIV) was used to measure the velocity field during a columnar/equiaxed solidification process. The single-phase measurement technique developed for PIV has been extended to cope with liquid-equiaxed flows. It was applied to NH₄Cl solidification in a die cast cell of 10*10*1 cm³ in which both the liquid velocity and the crystals velocity maps could be extracted. The separation between the two velocity fields could be obtained with the use of fluorescent tracer particles that emit different waves when excited with the laser wavelength. Two pictures were

taken simultaneously with two different cameras; the first one recorded only the laser light through a green filter, while the second one used an orange filter to record only waves emitted by the fluorescent particles. Thus the first camera could follow only the crystals paths, while the second camera recorded the liquid velocity field.

During the cooling down different regimes were observed. Before solidification, the flow is controlled by only thermal buoyancy. As soon as the solidification starts, turbulence and chaos are generated in the liquid due to solutal convection. In the same time strong equiaxed crystal rains occur at the vicinity of the solidification fronts. At the end of the process, the flow becomes steadier and auto-organizes in a meandering and stratified structure.

In general no clear relation was found between the size and the settling velocities of the crystals. However isolated crystals were found to fall much slower than spheres of equivalent apparent sizes, in agreement to what is generally believed. This fact could be explained due to the fractal crystal shape. For equiaxed crystals with diameters smaller than 1 mm, the drag coefficient was estimated to be 41.3.

The coupling between the fluid flow and the equiaxed crystal was found to be important in area of high crystal density. In these regions, the liquid flow has shown smoother velocity variations than in the chaotic or the turbulent bulk. This observation is a proof that equiaxed crystals tend to damp a part of the turbulence. Simultaneously the velocities in the bulk flow were found to accelerate during the period of strong crystal fall near the vertical walls. Perhaps in larger systems as in industrial scale a generation of turbulence could be observed. However in the present configuration, it is not yet clear how much is the contribution of the equiaxed rains to the generation of chaos with respect to the solutal buoyancy. Spatio-temporal behavior of the liquid and crystal flow suggested the presence of instabilities and auto-organization often observed in the field of nonlinear systems and chaos. This indicates that very complex behaviors can be expected from the interaction between flow and solidification in larger systems.

Acknowledgements

The research was funded by the Austrian Science Fund (FWF): P22614-N22.

References

- [1] Beckermann C and Viskanta R 1993 *Appl. Mech. Rev* **46** 1-27
- [2] Beckermann C 1993 *Int. Conf. Modeling of Casting, Welding and Advanced Solidification Processes VI* 'ed T S Piwonka et al' (Warrendale, Pennsylvania:TMS) pp 181-92
- [3] Rappaz M 1989 *Int. Mater. Rev.* **34** 93-123
- [4] Khalitov D A, Longmire E K 2002 *Exp. Fluids* **32** 252-68
- [5] Hassan YA, Schmidl W D and Ortiz-Villafuerte J 1998 *J. of Visualization* **1** 291-301
- [6] Delauré Y M C, Chan V S S and Murray D B 2003 *Exp. Thermal and Fluid Sci.* **27** 911-926
- [7] Skudarnov P V, Lin C X, Wang M H, Pradeep N and Ebadian M A 2002 *Int. J. of Heat and mass Transfer* **45** 5191-200
- [8] Appolaire B, Albert V, Combeau H and Lesoult G *ISIJ International* **39** 263-70
- [9] Appolaire B Ph.D. INPL 1999
- [10] Beckermann C and Wang C Y 1996 *Metall Mater TransA* **27** 2795-84
- [11] Rowe R C, Sheskey P J and Quinn M E 2009 *Handbook of Pharmaceutical Excipients* 6th ed. 'ed R C Rowe et al' (London, England: Pharmaceutical Press)
- [12] Badillo A, Ceynar D and Beckermann C 2007 *J. of Crystal Growth* **309** 197-215
- [13] Badillo A, Ceynar D and Beckermann C 2007 *J. of Crystal Growth* **309** 216-24
- [14] Appolaire B, Combeau H and Lesoult G 2008 *Mater. Sci. Eng. A* **487** 33-45
- [15] Wu M and Ludwig A 2009 *Acta Mater* **57** 5632-44